TUS

JOURNAL OF GEOPHYSICAL RESEARCH, VOL. 110, D06208, doi:10.1029/2004JD005480, 2005

# Vertical distribution of Saharan dust over Rome (Italy): Comparison between 3-year model predictions and lidar soundings

P. Kishcha
Department of Geophysics and Planetary Sciences, Tel Aviv University, Tel Aviv, Israel

F. Barnaba and G. P. Gobbi
Istituto di Scienze dell'Atmosfera e del Clima, CNR, Rome, Italy

P. Alpert, A. Shtivelman, S. O. Krichak, and J. H. Joseph
Department of Geophysics and Planetary Sciences, Tel Aviv University, Tel Aviv, Israel

Received 30 September 2004; accepted 24 November 2004; published 25 March 2005.

[1] Mineral dust particles loaded into the atmosphere from the Sahara desert represent one major factor affecting the Earth's radiative budget. Regular model-based forecasts of 3-D dust fields can be used in order to determine the dust radiative effect in climate models, in spite of the large gaps in observations of dust vertical profiles. In this study, dust forecasts by the Tel Aviv University (TAU) dust prediction system were compared to lidar observations to better evaluate the model's capabilities. The TAU dust model was initially developed at the University of Athens and later modified at Tel Aviv University. Dust forecasts are initialized with the aid of the Total Ozone Mapping Spectrometer aerosol index (TOMS AI) measurements. The lidar soundings employed were collected at the outskirts of Rome, Italy (41.84°N, 12.64°E) during the high–dust activity season from March to June of the years 2001, 2002, and 2003. The lidar vertical profiles collected in the presence of dust were used for obtaining statistically significant reference parameters of dust layers over Rome and for model versus lidar comparison. The Barnaba and Gobbi (2001) approach was used in the current study to derive height-resolved dust volumes from lidar measurements of backscatter. Close inspection of the juxtaposed vertical profiles, obtained from lidar and model data near Rome, indicates that the majority (67%) of the cases under investigation can be classified as good or acceptable forecasts of the dust vertical distribution. A more quantitative comparison shows that the model predictions are mainly accurate in the middle part of dust layers. This is supported by high correlation (0.85) between lidar and model data for forecast dust volumes greater than the threshold of $1 \times 10^{-12}$ $cm^3/cm^3$. In general, however, the model tends to underestimate the lidar-derived dust volume profiles. The effect of clouds in the TOMS detection of AI is supposed to be the main factor responsible for this effect. Moreover, some model assumptions on dust sources and particle size and the accuracy of model-simulated meteorological parameters are also likely to affect the dust forecast quality.

**Citation:** Kishcha, P., F. Barnaba, G. P. Gobbi, P. Alpert, A. Shtivelman, S. O. Krichak, and J. H. Joseph (2005), Vertical distribution of Saharan dust over Rome (Italy): Comparison between 3-year model predictions and lidar soundings, *J. Geophys. Res., 110*, D06208, doi:10.1029/2004JD005480.

## 1. Introduction

[2] The problem of climate changes and global warming has risen in importance during the past decades. In fact, the role of atmospheric aerosols on the climate system is found to be most significant [*Intergovernmental Panel on Climate Change*, 2001]. In this context, mineral dust particles loaded into the atmosphere from the Sahara desert certainly represent one major factor affecting the Earth's radiative budget. In particular, Saharan dust is a significant seasonal atmospheric phenomenon in the Mediterranean. Every year, from spring to autumn, mineral dust, produced by wind erosion over arid areas of North Africa, is transported away to the Middle East, over the Mediterranean to Europe, and across the Atlantic Ocean. These dust intrusions are considered as important because of their impact on weather conditions and ecosystems [*Prospero et al.*, 2002; *Israelevich et al.*, 2002,


0148-0227/05/2004JD005480$09.00

2003]. In particular, dust particles affect the atmosphere in two ways [e.g., *Kaufman et al.*, 2002; *Torres et al.*, 2002; *Ramanathan et al.*, 2001; *Rosenfeld*, 2002]: (1) by scattering and absorbing solar and thermal radiation (direct effect), thus reducing the solar irradiance at the Earth's surface, increasing the solar heating of the atmosphere, and affecting the atmospheric thermal structure and (2) by altering cloud microphysics, often leading to suppression of rainfall, and thus to a less efficient removal of aerosols from the atmosphere (indirect effect). The dust radiative effect strongly depends on its vertical location. Therefore knowledge on dust vertical distribution is of importance in determining the dust radiative effect in climate models. Besides, knowledge of dust vertical distribution is important for the reliable retrieval of aerosol optical depths from satellite observations [*Torres et al.*, 2002].

[3] Lidars are among the most efficient techniques for observing the vertical distribution of atmospheric aerosols with high vertical resolution. However, the Saharan dust lidar observations available in literature mainly refer to localized observations and case studies [*Hamonou et al.*, 1999; *Gobbi et al.*, 2000; *Di Sarra et al.*, 2001; *De Tomasi et al.*, 2003; *Müller et al.*, 2003]. To our knowledge, the yearly record of dust lidar profiles over Rome, recently analyzed by *Gobbi et al.* [2004], is the only long-term study of the vertical structure of dust layer.

[4] To fill the gaps in the observations of dust vertical profiles (generally spread in time and space), averaged 3-D fields of dust can be usefully obtained by regular model forecasts [e.g., *Alpert et al.*, 2004]. Of course, possible incorrect estimates of these 3-D distributions may add a bias to the model-predicted results. In order to feel confidence in the model's correctness, a comprehensive verification of model outputs should be made. In particular, a comparison of model results against lidar observations is believed to be very helpful to better understand the model's capabilities. Moreover, such a comparison could be a useful pilot study in using lidar-retrieved data for data assimilation and initialization of numerical short-term dust predictions. *Nickovic* [2003] has already discussed such a possibility for operational dust forecasting over the Euro-Mediterranean region by using the European Lidar Network (EARLINET) including about 20 stations. Now space missions equipped with lidar systems are being developed. So one can expect to obtain systematic space-borne lidar measurements soon (e.g., the NASA-CNES CALIPSO experiment, see http://www-calipso.larc.nasa.gov). In this respect, it is worth noting that the quantitative comparison between dust model outputs and lidar soundings is not straightforward. In fact, this comparison requires the conversion of the lidar-measured aerosol backscatter coefficient into the aerosol parameters, which are calculated by the model, typically dust concentration or dust volume. Recently, a method for estimating desert dust aerosol volume from lidar backscatter measurements was developed by *Barnaba and Gobbi* [2001]. A description of that method and discussion on the accuracy of lidar-derived dust volume estimates are given in sections 2.1.2 and 4.1, respectively. The *Barnaba and Gobbi* [2001] approach was used in the current study to derive height-resolved dust volumes from lidar measurements. The measurements over Rome, Italy (41.84°N, 12.64°E) collected in the 3-year period 2001–2003 were considered. With the purpose of verifying model dust forecasts, lidar-derived dust volume profiles were then quantitatively compared to the corresponding model predicted ones. The dust forecasts were produced by the Tel Aviv University (TAU) dust prediction system, which was initially developed at the University of Athens and later modified at Tel Aviv University [*Alpert et al.*, 2002]. The high dust activity season from March to June was selected for the model versus lidar comparison.

## 2. Methods

[5] A description of the lidar observations and of the method used for retrieving dust volume profiles from lidar soundings is given in this section together with the description of the TAU dust prediction system.

### 2.1. Lidar Observations

[6] Lidar measurements employed in this study were collected by a single-wavelength, polarization-sensitive lidar system (VELIS), operational since February 2001 in the ISAC laboratories (41.84°N–12.64°E, 130 m asl) at the outskirts of Rome. Measurements were carried out daily at nonsynchronous times between 0700 and 2100 (UTC), usually with 2–3 hourly intervals between measurements (observations are mainly performed during working days since the system is not automatic). Overall, a total of about 1000 profiles/year were collected, although some months are missing in the Rome 2002 and 2003 lidar records because of the system deployment in field campaigns.

#### 2.1.1. Lidar System and Lidar Signal Inversion

[7] The lidar was designed and assembled at the ISAC-Rome laboratories with the aim of creating a very compact system, capable of operating in both day and night conditions. The lidar radiation source is a frequency-doubled Nd:YAG laser, emitting plane-polarized pulses at 532 nm. The intensity and repetition rate of laser pulses are generally set as 30 mJ and 10 Hz, respectively. The system set up allows the collection of the complete tropospheric backscatter profile between 300 m and 14 km from the ground [e.g., *Gobbi et al.*, 2004]. Backscattered light is recorded on both the parallel and perpendicular polarization planes with respect to the laser one. Lidar profiles are obtained as 10-min averages and their vertical resolution is 37.5 m. A thorough description of the lidar signal analysis is given by *Gobbi et al.* [2002]. Retrieval of the aerosol backscatter is performed by numerically solving the elastic lidar equation [e.g., *Measures*, 1984]. A key point in such inversion is represented by the choice of the so-called "lidar ratio" ($L_r$), i.e., the ratio between aerosol extinction ($\sigma_a$) and backscatter ($\beta_a$), both appearing as unknowns in the single-wavelength lidar equation. In the VELIS lidar signal inversion, a vertically resolved, $\beta_a$-dependent lidar ratio $L_r = \sigma_a(z)/\beta_a(z)$ is chosen according to predetermined functional relationships ($\sigma_a = f(\beta_a)$). These were derived from numerical simulations performed for different aerosol models (maritime, desert dust continental) [*Barnaba and Gobbi*, 2001, 2004]. In particular, lidar profiles collected during Saharan dust events (as the ones discussed in this study) are inverted employing the desert dust extinction-to-backscatter relationship presented by *Barnaba and Gobbi* [2001] and taking into account particle nonsphericity following the inversion scheme

described by *Gobbi et al.* [2002]. Overall, this scheme has been proved to provide reliable backscatter and extinction profiles in dust load conditions [*Gobbi et al.*, 2002].

#### 2.1.2. Dust Detection and Retrieval of Dust Volume by Lidar

[8] The presence of dust is revealed by the lidar depolarization trace (D), which is highly effective at detecting the presence of nonspherical particles [*Gobbi et al.*, 2000]. The lidar depolarization D is here defined as the ratio between perpendicular and parallel polarized lidar signals ($D = S_{\perp}/S_{\parallel} \propto (\beta_{\perp a} + \beta_{\perp m})/(\beta_{\parallel a} + \beta_{\parallel m})$, where the subscripts "a" and "m" refer to aerosol and molecules, respectively). In fact, spherical particles as liquid aerosols do not generate a depolarized signal, whereas in the presence of nonspherical (solid) particles D levels markedly increase. In molecular (aerosol-free) scattering conditions our system detects $D \approx 1.4-2.0\%$ and similar low D values are found in the presence of spherical particles. Conversely, typical D values in the presence of desert dust range between 10 and 45%, depending on the relative, optically significant, impact of nonspherical particles on the total (aerosol plus molecules) backscattered signal (in lidar studies conveniently expressed in terms of backscatter ratio $R = (\beta_a + \beta_m)/\beta_m$, being $R = 1$ in a pure molecular atmosphere). The combination of both the backscatter ratio (R) and the depolarization information is therefore used to discriminate between dust (typically $D > 10\%$, $R > 1.5$) and nondust conditions (typically $D < 10\%$).

[9] The *Barnaba and Gobbi* [2001] approach used to derive the $\sigma_a = f(\beta_a)$ relationships (see section 2.1.1) was also employed to relate the lidar measured aerosol backscatter to other aerosol properties such as their surface area ($S_a$) and volume ($V_a$). These aerosol properties are important (1) to evaluate the aerosol capability to provide a substratum to chemical reactions and (2) to evaluate the aerosol load in the atmosphere. Functional relationship of the kind $V_a = f(\beta_a)$ were therefore derived as a tool to estimate macrophysical aerosol properties from a lidar measurement of backscatter. In particular, the desert dust $V_a = f(\beta_a)$ relationship (only derived for spherical particles) has been employed in this study to obtain lidar estimates of desert dust volume profiles to be compared to the TAU model ones. Following this scheme, the minimum dust volume detectable by the VELIS lidar is $1.0 \times 10^{-12}$ cm$^3$/cm$^3$, while the maximum dust volume is $1.0 \times 10^{-8}$ cm$^3$/cm$^3$. Discussion on the error expected to affect such lidar-derived desert dust volume estimates is given in section 4.1.

### 2.2. TAU Dust Prediction System

[10] The dust prediction system was initially developed at the University of Athens (S. Nickovic et al., Aerosol production/transport/deposition processes in the Eta model: Desert cycle simulations, preprint, Proceedings of the Symposium on Regional Weather Prediction on Parallel Computer Environments, University of Athens, Athens, Greece, 1997, hereinafter referred to as Nickovic et al., preprint, 1997). After modification the system has been put in operational use for short-term dust predictions at Tel Aviv University since November 2000 [*Alpert et al.*, 2002]. Results of the daily model predictions are available at http://earth.nasa.proj.ac.il/dust/current/. The forecasting model with its dust package and initialization procedure have already been discussed in detail in several publications [*Janjic*, 1990; *Nickovic and Dobricic*, 1996; *Nickovic et al.*, 1997; *Tsidulko et al.*, 2002; *Alpert et al.*, 2004; *Krichak et al.*, 2002]. Nevertheless, for the reader's convenience the following main features are worth outlining.

[11] The system is based on the hydrostatic NCEP Eta eta vertical coordinate model [*Mesinger*, 1997]. The model domain is 0°–50°N, 50°W–50°E including the tropical North Atlantic Ocean, North Africa, the Middle East, and the Arabian Peninsula. The model is initialized with the NCEP analysis and the lateral boundary data are updated every 6h, from the operational forecasts by the NCEP global model. The runs start at 1200 UTC and forecasts are performed for 3-hour periods up to 48 hours.

[12] The model includes packages for dust initialization, transport, and wet/dry deposition, which had been developed at the University of Athens within the framework of the Mediterranean Dust Experiment (MEDUSE) EU project [*Nickovic and Dobricic*, 1996; *Janjic*, 1990; Nickovic et al., preprint, 1997]. The dust mobilization scheme takes into account the values of the friction and threshold friction velocity, soil wetness and the distribution of the dust source areas, which are specified according to the Olson World Ecosystem data set [*Olson et al.*, 1985]. The set contains 59 classes of vegetation with 10′ resolution. Dust forecasts are initialized with the aid of the Total Ozone Mapping Spectrometer aerosol index (TOMS AI) measurements [*Alpert et al.*, 2002]. The initial dust vertical distribution over each grid point within the model domain is determined according to the value of TOMS indices among four categories of model-calculated averaged dust profiles over the Mediterranean and among four other profiles over North Africa. The four profiles correspond to the average model output profiles at four respective TOMS AI domains of 0.7–1.1, 1.1–1.5, 1.5–1.9, and > 1.9. Some additional comments about the TOMS initialization can be seen in section 4.2.2.

[13] All the dust (clay) particles were assumed to be of the same effective radius of 2–2.5 microns. This choice remained in the model for all period of its operational use without changes. Hence all model results used in this study are homogeneous. We understand, however, that the single-size aerosol is a major shortcoming of the TAU model version, and we are currently experimenting with a number of aerosol sizes (see section 4.2). The dust is considered as a passive substance. No dust feedback effects are included in the radiation transfer calculations. The feedback, however, could be an important factor in the energy balance, because of dust radiative effects, as mentioned in section 1. This is especially important as, according to lidar measurements (section 3.1), dust layers over Rome are rather thick; their averaged thickness exceeds 3 km. Unfortunately, the model does not take the dust feedback into account. The effect of such feedback on the vertical distribution of dust is not well understood and is currently under investigation.

[14] The database of model outputs contains a 3-year daily data set of 48-hour forecasts, obtained for 3-hour periods, and is available from November 2000 up to the present. The data are 2-D and 3-D fields of several atmospheric parameters including dust loading, dust concentration, three wind components, temperature, geopotential heights, sea level pressure and specific humidity. Horizontal resolution of the model is 0.5° and its vertical resolution is

**Table 1.** Number of Dusty Days Over Rome Averaged Monthly as Derived by Both TOMS and Lidar Data[a]

| Month | Number of Dusty Days Over Rome | |
|---|---|---|
| | TOMS 1979–1993 | Lidar 2001–2003 |
| January | 3.4 ± 2.4 | 0.5 ± 0.7 |
| February | 3.3 ± 2.4 | 0.3 ± 0.6 |
| March | 5.6 ± 3.7 | 7.0 ± 4.6 |
| April | 6.9 ± 3.2 | 3.3 ± 2.1 |
| May | 7.0 ± 3.5 | 8.3 ± 3.0 |
| June | 5.6 ± 3.1 | 6.7 ± 0.6 |
| July | 5.8 ± 2.7 | 6.0 |
| August | 4.2 ± 1.8 | - |
| September | 2.7 ± 1.7 | 0.5 ± 0.7 |
| October | 2.1 ± 1.6 | 5.0 ± 4.6 |
| November | 1.9 ± 2.3 | 4.7 ± 1.5 |
| December | 2.3 ± 2.4 | 1.3 ± 2.3 |

[a]Total Ozone Mapping Spectrometer (TOMS) averages were computed for TOMS aerosol index > 0.2 over the domain (41°N–43°N, 12°E–14°E) around Rome for the 15-year period 1979–1993. The lidar-derived values were averaged monthly over the period 2001–2003.

32 model levels. To compare the dust forecast with lidar-derived volume profiles, modeled mass concentration profiles over Rome were divided by dust density, assumed as 2.5 g/cm$^3$ (in agreement with the majority of other dust models [e.g., *Kinne et al.*, 2003, Table 4]).

## 3. Results

[15] In this section an overview of the dust load over Rome is given first, followed by the model-lidar comparison of dust vertical profiles.

### 3.1. Statistics of Dusty Day and Dust Layer Characteristics in Rome

[16] Dust from the Sahara desert is observed irregularly over Rome. In the beginning, it is therefore important to estimate the mean number of dusty days usually registered at the Rome site during the year. The TOMS AI was used to produce these estimates. By definition, AI is positive for absorbing aerosols, it is $-0.2 < AI < 0.2$ in the presence of clouds, while negative AI are found for nonabsorbing particles [*Torres et al.*, 2002]. The threshold $AI > 0.2$ was selected to identify dusty conditions. Owing to some technical problems with the Earth Probe TOMS instrument, the TOMS aerosol indices for the 15-year period 1979–1993 are of better quality than the ones retrieved after November 2000 (available at http://toms.gsfc.nasa.gov/aerosols/aerosols_v8.html). Therefore the TOMS data from 1979 to 1993 were used in order to get a reliable statistics of the mean number of dusty days in Rome.

[17] In Table 1 is reported the number of dusty days (N), averaged on a monthly basis over a small domain (41°N–43°N, 12°E–14°E) around Rome. One can see that the maximum, $N \sim 7$ days, is registered in April–May while the minimum, $N < 2$ days, is registered in November. In addition, a comparison between TOMS-based statistics and lidar-derived ones is also shown in Table 1. Although some differences with the lidar-based statistics are found in the winter and autumn months, this comparison shows a general good agreement between the lidar and TOMS data during the season under investigation in the current study (March–June). In fact, both the lidar and TOMS data show a

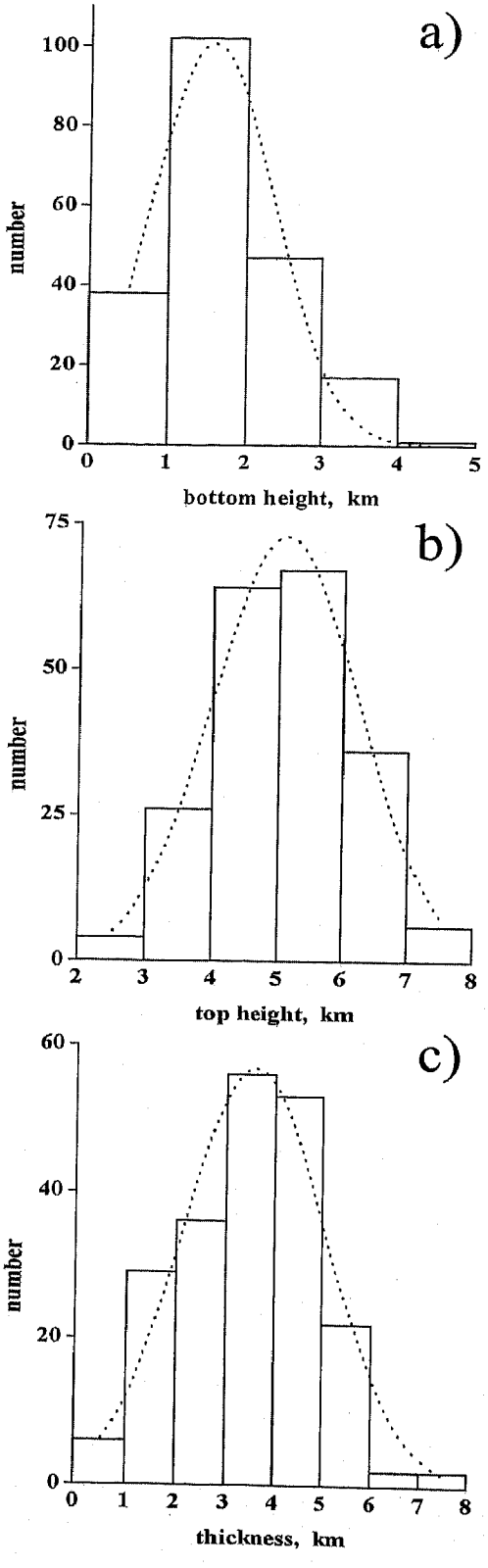


**Figure 1.** Statistical distributions of lidar-derived parameters of the dust layer over Rome based on the March-to-June data set of dust-affected lidar profiles (206): (a) bottom and (b) top heights (km), and (c) thickness (km). Fitting curves of the Gaussian distribution are shown by dotted lines.

Table 2. Dust Layer Parameters Over Rome Retrieved From Lidar Remote Soundings During March–June 2001–2003, Model-Calculated Dust Volumes, and the Type of Correspondence Between Lidar and Model Volume Profiles[a]

| | Date[b] | Time, UTC | Hbot, km | Htop, km | Thick, km | V1ave, $10^{-12}$ cm$^3$/cm$^3$ | V2ave, $10^{-12}$ cm$^3$/cm$^3$ | V1max, $10^{-12}$ cm$^3$/cm$^3$ | V2max, $10^{-12}$ cm$^3$/cm$^3$ | Type |
|---|---|---|---|---|---|---|---|---|---|---|
| | | | | | *March* | | | | | |
| 1 | 010316 | 18.02 | 1.2 | 4.2 | 3 | 5.28 | 3.78 | 7.74 | 5.00 | II |
| 2 | 020304 | 9.30 | 1.8 | 2.7 | 0.9 | 6.04 | 0.04 | 11.60 | 0.06 | IV |
| 3 | 020305 | 12.00 | 0.5 | 5.5 | 5.0 | 5.81 | 0.51 | 19.40 | 0.90 | II |
| 4 | 020306 | 11.21 | 1.7 | 4.2 | 2.5 | 3.62 | 7.65 | 4.90 | 12.37 | II |
| 5 | 020307 | 11.03 | 1.2 | 6.5 | 5.3 | 6.69 | 0.15 | 14.50 | 0.40 | IV |
| 6 | 020315 | 11.35 | 1.2 | 5 | 3.8 | 132.00 | 0.11 | 703.00 | 0.38 | IV |
| | | | | | *April* | | | | | |
| 7 | 020409 | 7.33 | 1.4 | 4.5 | 3.1 | 25.80 | 19.74 | 38.80 | 28.08 | I |
| 8 | 020412 | 12.23 | 0.5 | 4.5 | 4.0 | 87.40 | 95.00 | 206.00 | 133.15 | I |
| 9 | 030430 | 14.30 | 0.5 | 5.5 | 5.0 | 8.89 | 5.61 | 15.10 | 8.28 | I |
| | | | | | *May* | | | | | |
| 10 | 010502 | 12.15 | 3.0 | 5.4 | 2.4 | 9.74 | 0.17 | 17.50 | 0.88 | III |
| 11 | 010503 | 12.16 | 2 | 6 | 4 | 19.30 | 0.52 | 41.80 | 1.00 | II |
| 12 | 010516 | 12.42 | 3.0 | 4.6 | 1.6 | 5.23 | 0.04 | 9.11 | 0.09 | IV |
| 13 | 010517 | 11.05 | 1.2 | 6 | 4.8 | 7.03 | 0.08 | 12.00 | 0.10 | II |
| 14 | 010518 | 15.56 | 0.5 | 6 | 5.5 | 7.46 | 0.90 | 40.30 | 1.31 | II |
| 15 | 010521 | 16.13 | 0.5 | 6.8 | 6.3 | 12.80 | 8.96 | 31.90 | 18.83 | I |
| 16 | 010523 | 14.42 | 0.5 | 5 | 4.5 | 50.01 | 5.06 | 409.00 | 20.67 | II |
| 17 | 020507 | 19.33 | 1.4 | 5.5 | 4.1 | 9.83 | 9.18 | 23.40 | 14.19 | I |
| 18 | 020509 | 19.05 | 1.5 | 5 | 3.5 | 4.06 | 5.80 | 11.50 | 15.57 | I |
| 19 | 020510 | 16.30 | 0.5 | 6 | 5.5 | 17.30 | 1.23 | 43.60 | 1.79 | II |
| 20 | 020522 | 14.51 | 3 | 4 | 1 | 3.68 | 1.76 | 7.98 | 1.79 | III |
| 21 | 020523 | 12.06 | 1.5 | 5.4 | 3.9 | 52.20 | 0.32 | 135.00 | 0.89 | IV |
| 22 | 030505 | 10.10 | 0.5 | 4 | 3.5 | 10.70 | 11.32 | 56.20 | 16.49 | III |
| 23 | 030508 | 12.27 | 1.2 | 5.5 | 4.3 | 32.50 | 35.46 | 212.00 | 59.94 | I |
| 24 | 030512 | 13.36 | 1.2 | 4.8 | 3.6 | 7.54 | 10.03 | 18.60 | 14.37 | I |
| 25 | 030526 | 10.45 | 1 | 5 | 4 | 10.30 | 6.98 | 27.90 | 12.83 | I |
| | | | | | *June* | | | | | |
| 26 | 010611 | 9.00 | 1.2 | 6 | 4.8 | 11.40 | 12.24 | 37.50 | 16.70 | I |
| 27 | 010612 | 10.24 | 1.8 | 7 | 5.2 | 11.80 | 0.81 | 80.20 | 1.10 | I |
| 28 | 010613 | 9.13 | 0 | 5.4 | 3.4 | 11.30 | 7.88 | 29.80 | 12.40 | I |
| 29 | 010628 | 16.00 | 0.5 | 4.6 | 4.1 | 14.80 | 3.10 | 28.20 | 6.71 | II |
| 30 | 020604 | 15.20 | 1.8 | 6.4 | 4.6 | 9.65 | 11.76 | 19.80 | 25.20 | I |
| 31 | 020605 | 10.24 | 1.4 | 5.0 | 3.6 | 163.00 | 34.13 | 1830.00 | 44.20 | IV |
| 32 | 020628 | 12.23 | 1.4 | 5.7 | 4.3 | 11.00 | 4.43 | 14.80 | 10.62 | III |
| 33 | 030625 | 14.28 | 1.8 | 5.5 | 3.7 | 16.80 | 6.84 | 32.90 | 9.86 | II |
| 34 | 030627 | 12.42 | 1.5 | 5.6 | 4.1 | 10.50 | 1.53 | 18.40 | 5.44 | III |

[a]Definitions are as follows: Hbot, bottom altitude of dust layer; Htop, top altitude; Thick, thickness; V1ave (V1max) and V2ave (V2max), average (maximum) dust volume from lidar and model data, respectively.
[b]Format is year, month, and day; read, for example, 010316 as 16 March 2001.

maximum from March to June. Even though the monthly mean numbers of dusty days are not coincident during this period, they are within the associated error bars.

[18] Specific atmospheric conditions, accompanied by dust transport from North Africa to the central Mediterranean, lead to the results of Table 1. Saharan dust is generally transported over the Mediterranean by southerly winds generated by cyclones [*Alpert and Ziv*, 1989; *Alpert et al.*, 1990; *Bergametti et al.*, 1989; *Moulin et al.*, 1998]. In particular, *Alpert and Ziv* [1989] found that spring and early summer are the most favorable periods for the development of Saharan lows (also called Sharav cyclones) south of the Atlas Mountains. Usually, such cyclones move eastward and cross Egypt, Israel and the eastern Mediterranean basin. As shown by *Bergametti et al.* [1989], *Moulin et al.* [1998], dust outbreaks to the western and central parts of the Mediterranean are linked with two depression centers: Saharan lows and a high over Libya. The high over Libya prevents Saharan lows from following an eastward direction. This synoptic situation, having a peak in spring and in early summer, induces strong south and southwestern winds between the two systems and is characterized by dust intrusions from North Africa to the Mediterranean basin. Moreover, complex wind fields associated with frontal zones under those atmospheric conditions could be one of the causal factors for dust over Rome being within a wide range of altitudes, penetrating high into the troposphere.

[19] As mentioned in section 1, there is little information about dust vertical distribution. Therefore the data set of regular VELIS-lidar soundings is important in obtaining reference values of dust layers over Rome. On the basis of the whole data set of dust-affected lidar profiles (206) in the period March–June (2001–2003), Figure 1 presents histograms of the main parameters of these dust layers. In particular, the bottom boundary (BT) was found to range from 0.5 km to 5 km, with the mean value BT = 1.6 ± 0.8 km;

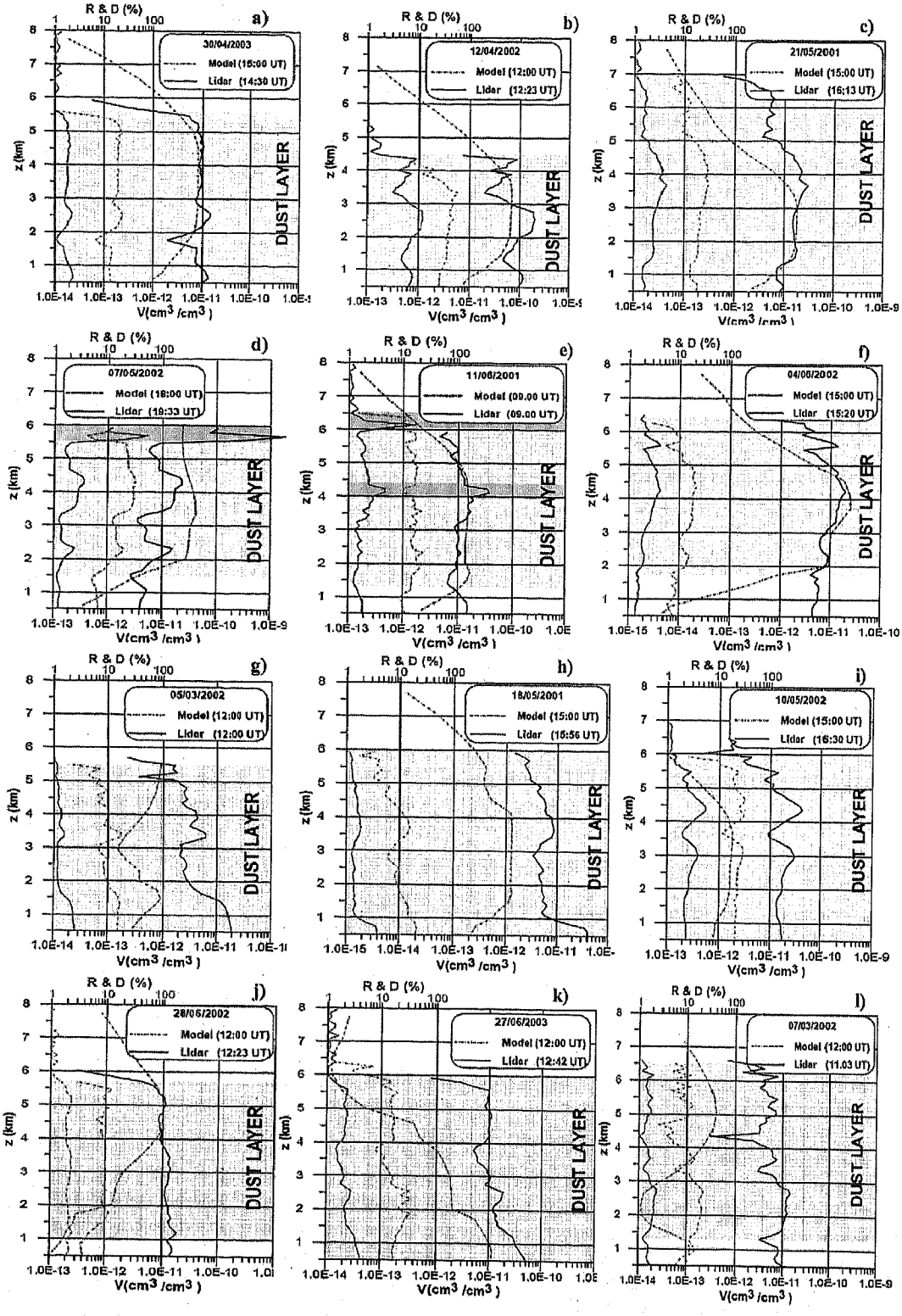


**Figure 2.** (a–l) Examples of dust volume profiles over Rome from March to June used in the model-lidar comparison. The solid lines designate the lidar profiles, while the dashed lines designate the model profiles. For completeness, relevant lidar profiles of both backscatter ratio (R) (solid gray line) and depolarization (D) (dashed gray line) are also presented. Shaded areas indicate the vertical extension of the dust layers. Horizontal gray bands in Figures 2d and 2e indicate cloud layers.

the top boundary (TP) ranges from 2.4 to 8 km, with mean value TP = 5.1 ± 1.1 km, and the thickness of dust layers (TH) ranges from 0.4 km to 7.5 km, with mean value TH = 3.6 ± 1.5 km. Hence, on average, dust over Rome is distant from the surface. Nonetheless, some mixing of dust with local (typically liquid) aerosols below the dust layer bottom boundary is often highly probable, thus making its detection more difficult (see also section 4.1). In Figure 1, Gaussian fitting curves of each variable (dotted lines) are also shown. One can see that these Gaussian distributions suit the histograms of lidar-derived data. In seasons other than March–June, some indication of the mean vertical distribution of dust over Rome are given by *Gobbi et al.* [2004], based on lidar data collected in the year 2001.

### 3.2. Model-Lidar Dust Volume Comparison

[20] Saharan dust-affected profiles collected over Rome from March to June 2001–2003 were considered for the analysis. Out of the 69 days in which the lidar detected dust, a database of 34 days was selected for the lidar versus model comparison. In fact, only days with both the lidar observations and the model forecast could be taken into account. In particular, there were no model runs for 8 days because of technical problems. Some days (27) with low dust loading (TOMS AI less than 1) could not be used because of the restriction in model dust forecasts. It is worth mentioning that, in such cases, dust was observed by lidar within thin layers (average thickness of TH = 2.7 ± 1.1 km) with respect to the general mean value (TH = 3.6 ± 1.5 km). In these circumstances, the low value of TOMS AI could be explained by the concurrent presence of nonabsorbing anthropogenic aerosols in the atmospheric column and/or reflecting clouds (see also section 4.2). It should also be mentioned that the lidar dust record is partly limited by the presence of dense clouds. In fact, since Mediterranean dust transport is often associated with meteorological fronts, dust layers are frequently associated with water clouds, making the lidar soundings inefficient in characterizing the dust vertical distribution.

[21] The resulting list of dates employed for the model versus lidar comparison is given in Table 2, where corresponding lidar and model estimates of dust volume are also reported. Since this study was aimed at checking the quality of dust forecasts available daily at 1200 UTC, the lidar dust profiles closest to 1200 UTC were selected for the analysis. However, for those few cases when lidar profiles were available only in the evening or in the morning (e.g., 16 March 2003, 7 May 2002, 9 May 2002), the dust forecast closest to the lidar measurements (either a 21-hour or a 30-hour forecast) was selected for the analysis.

[22] In order to classify the model-lidar agreement, four different categories (I–IV) have been defined as listed below. (For each category, examples are provided in Figure 2): category I, the model profile corresponds well to the lidar one in the altitude range 1.6–5.1 km (i.e., in the altitude range within the mean dust bottom and the mean dust top) (see Figures 2a–2f); category II, the model and lidar profiles do not coincide but are similar in shape (Figures 2g–2i); category III, only a part of the model profile (e.g., the top or the bottom of dust layers) fits the lidar sounding (Figures 2j and 2k); and category IV, the model profile does not fit the lidar one at all (Figure 2l). As also indicated in Table 2, 13 cases (38%) belong to category I, even though the model usually underestimates dust volume derived from the lidar sounding. Category II is also considered to be tolerable; 10 cases (29%) fall into this category. Five cases (15%) fall into categories III, while six cases (18%) fall into category IV. It can be observed that, representing 67% of all cases, categories I and II (i.e., accurate and acceptable forecasts) are prevalent here.

[23] Note that the discrepancies between lidar and modeled profiles registered at the lower levels (z < 2 km) in Figure 2 are partially due to the presence in this region of boundary layer aerosols (mainly of local origin) measured by the lidar but not simulated by the dust model. This point is further commented on in section 4.1.

#### 3.2.1. Case Studies

[24] As examples of the above mentioned categories, three specific cases will be discussed in the following. The purpose is to illustrate how different atmospheric conditions lead to the dust profile observed over Rome and affect the model capability to reproduce it.

##### 3.2.1.1. The 12 April 2002 Case

[25] Shown in Figure 2b, this case can be classified as a category I forecast. In fact, the model-predicted dust volume profile well coincides with the lidar-derived one. The NCEP-based map of sea level pressure, shown in Figure 3a, demonstrates the intensive low centered over the western Mediterranean with the central pressure as low as 996 hPa. One can see that the western and the central Mediterranean were dominated by low pressure while high pressure was observed over the eastern Mediterranean. This low was also well developed at the geopotential height of 500 hPa (not shown) with the central minimum value ~5380 m over southeastern Spain. The low significantly affects North Africa as also revealed by the wind distribution at 850 hPa (Figure 3b). Strong airflow with speeds higher than 20 m/s was observed at 500 hPa pressure level directed from North Africa to Italy (not shown). Such a synoptic situation produced favorable conditions for the development of the heavy dust storm over North Africa. This dust storm was accompanied by an intensive dust intrusion into the central Mediterranean and southern Europe. Figure 3c presents the SeaWiFS image of the Mediterranean area on the day previous to the forecast (see http://www.nrlmry.navy.mil/aerosol/satellite/seawifs/med/). One can see two significant cloud systems: one over Spain and another between southern Italy and Libya. Dust is seen in the passage between these cloud systems (it is clearly seen in the original true-color SeaWiFS image, but unfortunately it is not so clear in this gray scale one). The 24-hour air mass backward trajectories (Figure 3d) show that air masses, reaching Rome at the bottom, the middle and the top heights of the lidar-derived dust layer on 12 April were advected from Algeria/Tunisia within the passage between cloud systems. The trajectories were obtained by means of the HYSPLIT model via NOAA ARL READY Website (available at http://www.arl.noaa.gov/ready/hysplit4.html). Large values of TOMS AI (about 3.5) were observed in the area around the endpoints of 24-hour air mass backward trajectories (see Figures 3d and 3e). The 48-hour predicted evolution of dust concentration over Rome as a function of time and altitude is

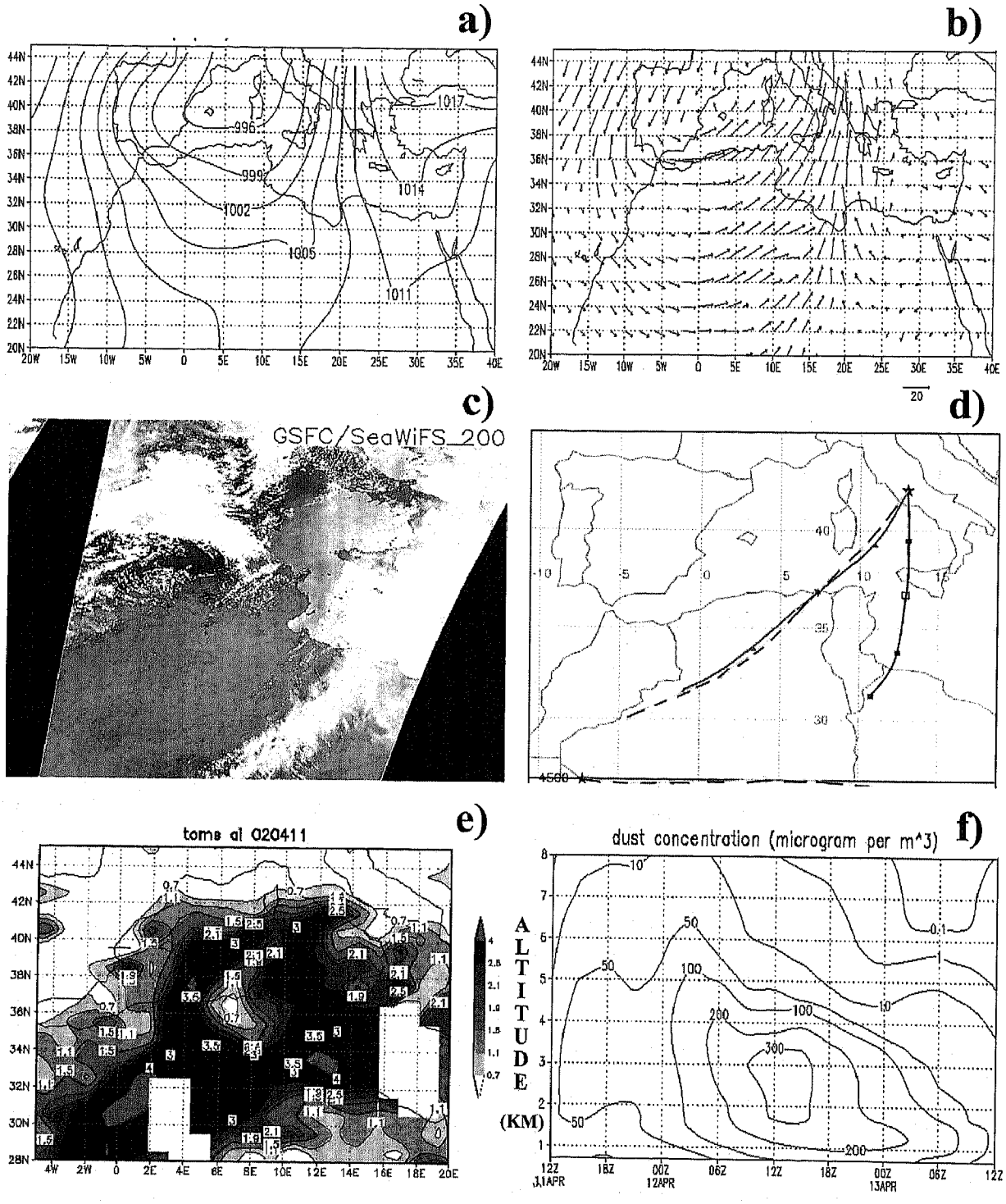


**Figure 3.** The National Centers for Environmental Prediction (NCEP)-based maps of atmospheric parameters: (a) sea level pressure (hPa); (b) wind at 850 hPa pressure level (m/s), (c) SeaWiFS image of the Mediterranean area on the day previous to the forecast, (d) 24-hour air mass back trajectories starting over Rome (at the bottom, middle, and top heights of the lidar-measured dust layer), (e) horizontal distribution of Total Ozone Mapping Spectrometer (TOMS) aerosol index (AI) on the day previous to the forecast, (f) predicted evolution of dust concentration ($\mu g/m^3$) over the domain (41°N–43°N, 12°E–14°E) around Rome on 12 April 2004.

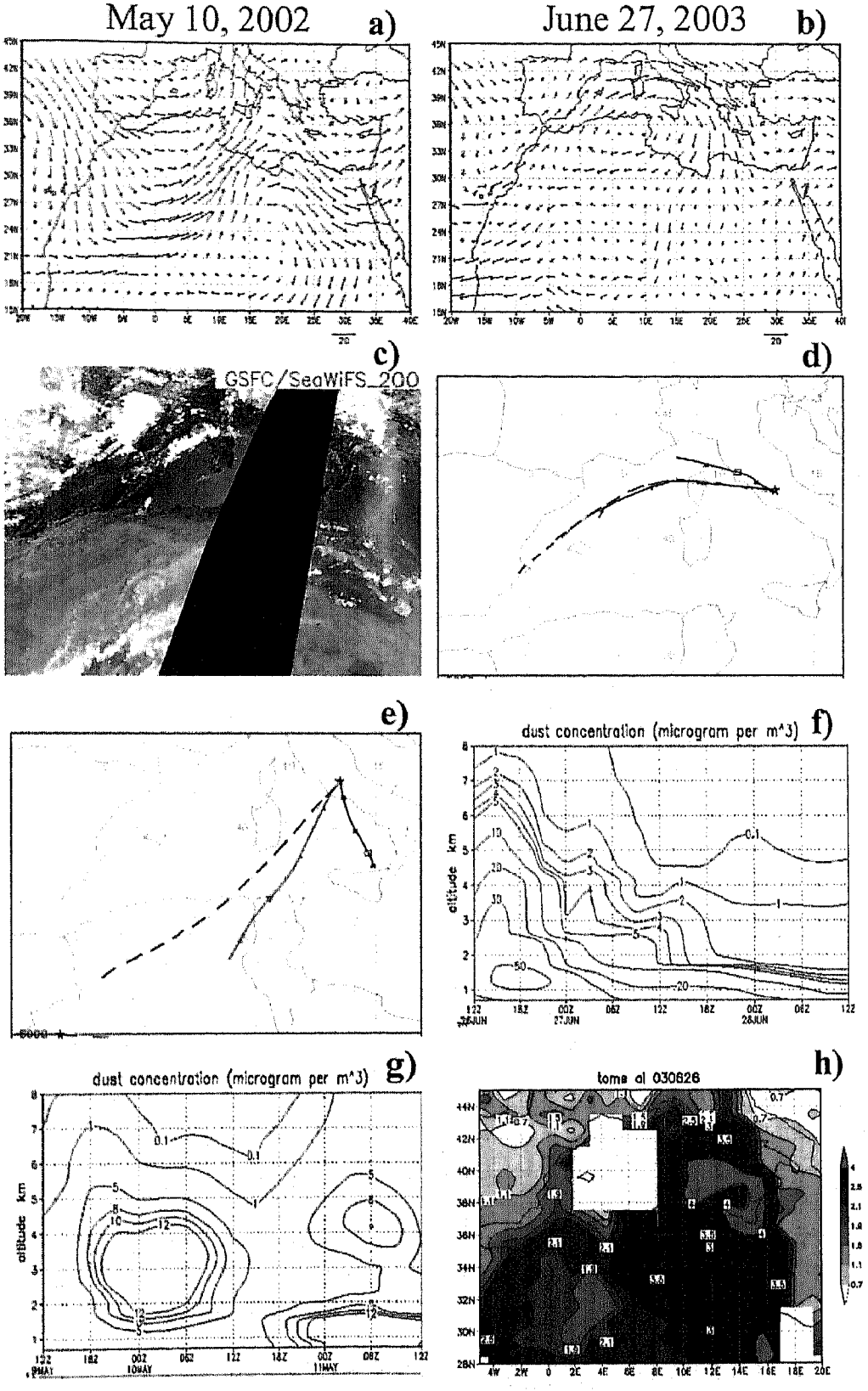


**Figure 4.** (left) The 10 May 2002 and (right) 27 June 2003 cases: (a and b) NCEP-based maps of wind at 700 hPa pressure level (m/s), (c) SeaWiFS image of the Mediterranean area on the day previous to the forecast (9 May 2002), (d and e) 24-hour air mass back trajectories starting over Rome (at the bottom, middle, and top heights of the lidar-measured dust layer), (f and g) 48-hour Tel Aviv University model-predicted evolution of dust concentration ($\mu g/m^3$) over the domain (41°N–43°N, 12°E–14°E) around Rome, and (h) horizontal distribution of TOMS AI on the day previous to the forecast (26 June 2003).

displayed in Figure 3f. One can see the largest values of dust concentration are predicted between 1.5 and 4 km on 12 April around noon.

### 3.2.1.2. The 10 May 2002 Case

[26] This case was classified as an acceptable forecast (category II, Figure 2i). The synoptic situation on 10 May 2002 was characterized by the African cyclone with the central pressure dropped to less than 1010 hPa over Algeria/Tunisia. The appropriate distribution of wind at 700 hPa shows ordered airflow from North Africa to Italy (Figure 4a). There was only a few clouds on the day previous to the forecast (9 May 2002), in accordance with the SeaWiFS image (Figure 4c). Presented in Figure 4e, the 24-hour backward trajectories show that the air masses reaching Rome at different altitudes follow different trajectories from Algeria/Tunisia and from the Mediterranean area. Figure 4g shows the 48-hour model-predicted evolution of dust concentration over Rome. One can see that this dust transport occurred in "pulses." One can suggest that the timing of dust pulses on 10 May 2002 was not sufficiently correct in the model output. As a result, the model volume profile at 1500 UTC does not coincide exactly with the profile derived from the lidar sounding at 1630 UT.

### 3.2.1.3. The 27 June 2003 Case

[27] Shown in Figure 2k, this case belongs to category III because only the bottom part of the model profile fits approximately the lidar soundings. The NCEP-based map of sea level pressure (not shown) demonstrates the low centered over the western Sahara. The cyclonic airflow near the surface is, however, replaced by the anticyclonic airflow at 850 hPa and higher (see the wind distribution at 700 hPa in Figure 4b). Such a synoptic situation produced favorable conditions for the intensive dust intrusion into the Atlantic Ocean. Nevertheless, the anticyclonic airflow over northwest Africa at 700–850 hPa could be also responsible for dust intrusion into the western part and subsequently into the central part of the Mediterranean region. The 24-hour air mass backward trajectories support this assumption (Figure 4d). Presented in Figure 4f, the 48-hour predicted evolution of dust concentration over Rome indicates a descending dust layer having the maximum concentration close to the surface and decreasing with time. However, the lidar-derived profiles showed the dust layer between 1.5 and 5.6 km with approximately the same dust volume at all altitudes (see Table 2 and Figure 2k). The discrepancy can be partly explained by some technical problems with TOMS detection of aerosol indices on the day previous to the forecast (26 June 2003). According to the horizontal distribution of TOMS AI displayed in Figure 4h, data were not

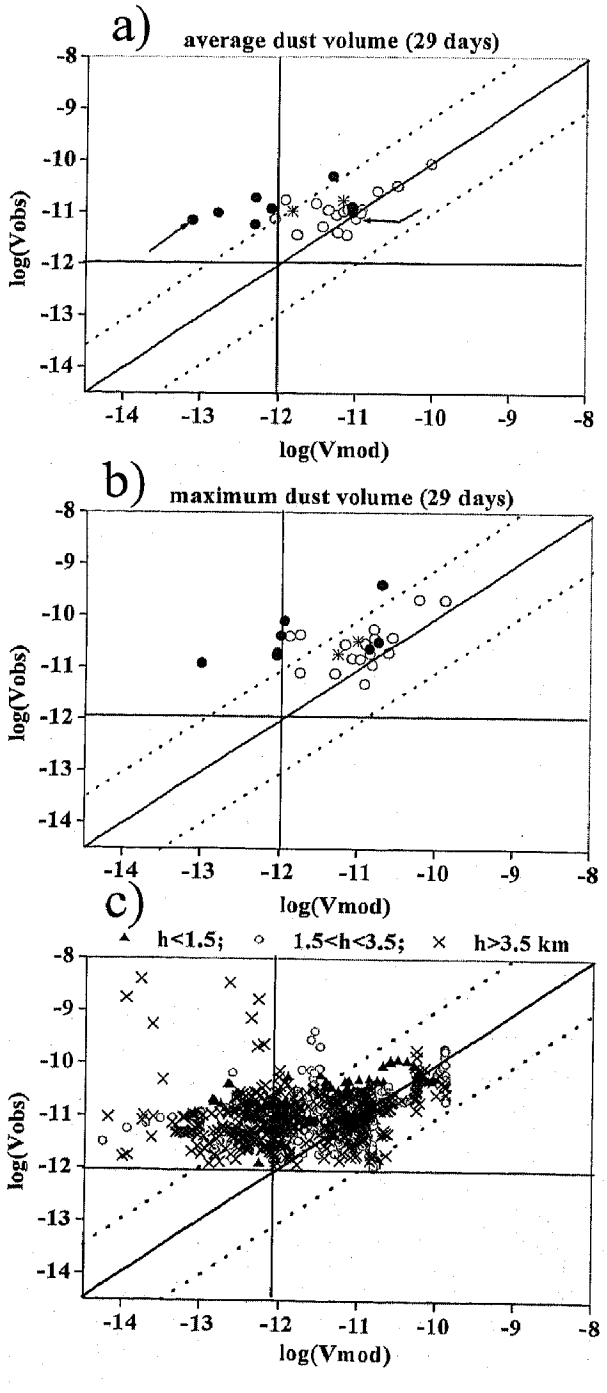


**Figure 5.** The scatterplots between the common logarithm of model-simulated dust volumes (Vmod) ($cm^3/cm^3$) over Rome and the ones retrieved from lidar soundings (Vobs): (a) averaged dust volume within the dust layer, (b) maximum dust volume within the dust layer, and (c) dust volumes at different altitudes along the dust profiles. Dashed lines show the root-mean-square intervals of deviations from the bisector. In Figures 5a and 5b the open circles correspond to the points with the averaged TOMS reflectivity less than 20%, while the solid circles correspond to points with the averaged TOMS reflectivity greater than or equal to 20%. The stars display 2 days when TOMS reflectivity measurements were not available. In Figure 5c the triangles designate dust volume at altitudes below 1.5 km, the circles designate dust volume between 1.5 and 3.5 km, and the crosses designate dust volume above 3.5 km. The horizontal solid lines, intersecting the vertical axis (lidar data) at $1 \times 10^{-12}$ $cm^3/cm^3$, correspond to the minimum dust volume detectable by the lidar. The vertical solid lines, intersecting the horizontal axis (model data) at $1 \times 10^{-12}$ $cm^3/cm^3$, correspond to a threshold of trustworthy dust forecasts. The arrows in Figure 5a indicate two points analyzed in section 3.2.2.

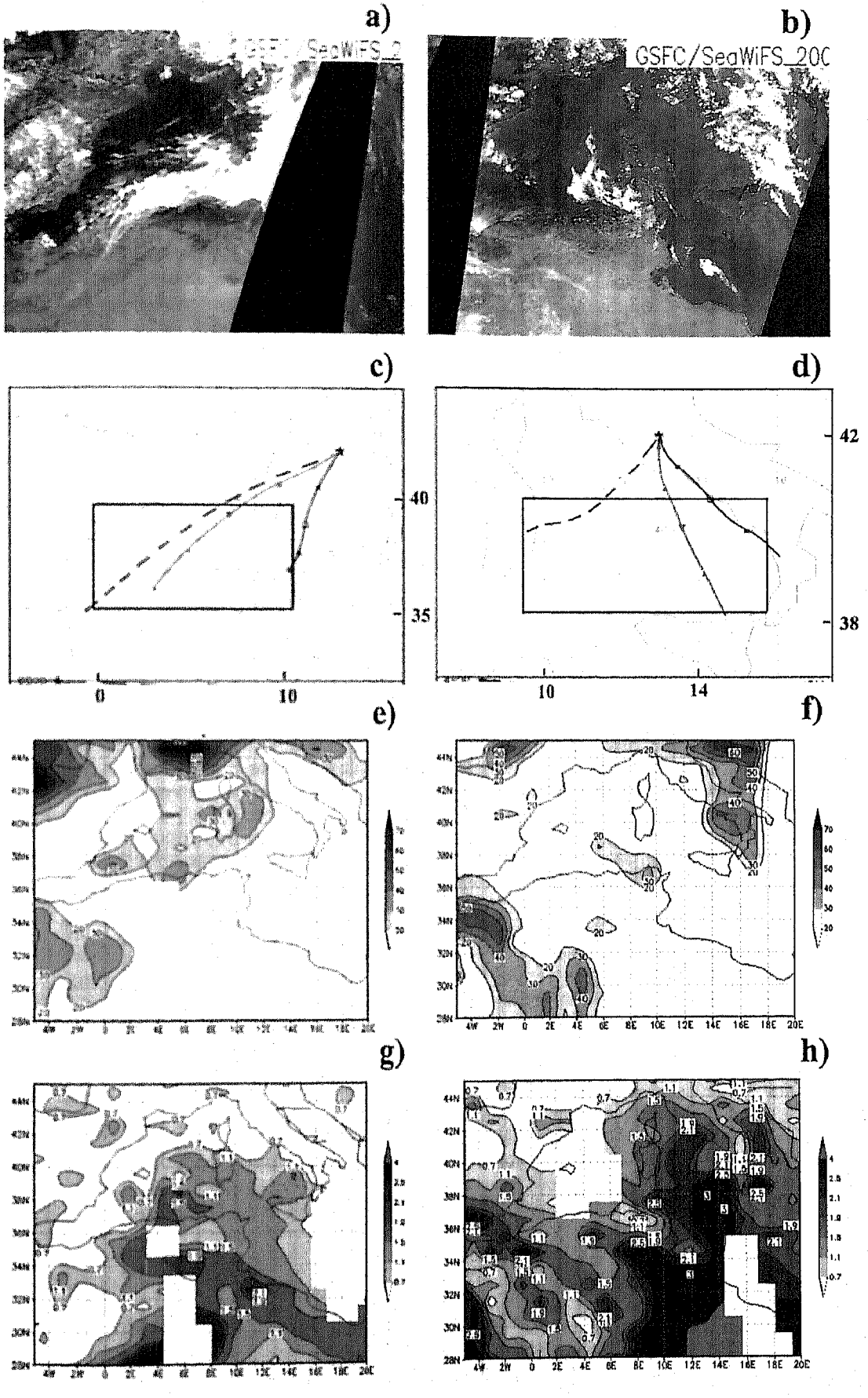


Figure 6

available over the area crossed by the air mass trajectories responsible for the middle and top parts of the dust layer over Rome.

### 3.2.2. Quantitative Intercomparison

[28] The qualitatively defined categories listed in section 3.2 stimulated interest in quantitatively evaluating the model versus lidar correspondence. As a matter of fact, only a quantitative comparison can validate the forecast of 3-D distribution of Saharan dust over the model domain. Among the 34 dusty days listed in Table 2, a quantitative comparison was only performed for the 29 days belonging to categories I–III. It is clear that the results of the quantitative comparison would deteriorate with the inclusion of the six category IV profiles.

[29] The correspondence between model data and lidar measurements is evaluated by means of scatterplots. For this purpose, lidar-derived (Vobs) versus model-simulated (Vmod) dust volumes are shown in Figure 5. Three different parameters of the dust vertical distribution are analyzed in Figure 5: (1) the averaged dust volume within the dust layer (Figure 5a), (2) the maximum dust volume within the dust layer (Figure 5b), and (3) dust volume at standard altitudes with vertical resolution 0.1 km, obtained by spline interpolation from available model and lidar profiles (Figure 5c). In Figure 5, the bisector indicates ideally accurate forecasts; that is, the points on or close to the bisector represent the best correspondence between the model-simulated data and the lidar ones. The root-mean-square intervals of deviations of points from the bisector (the dashed lines in Figure 5) can be used in order to characterize the range of forecast accuracy.

[30] The distribution of points in the scatterplot in Figure 5a reveals that the model results vary between $10^{-14}$ $cm^3/cm^3$ and $10^{-10}$ $cm^3/cm^3$, whereas the lidar data are between the lower detection limit of $10^{-12}$ and $10^{-10}$ $cm^3/cm^3$. One can see, however, that nearly all points to the right of the vertical line (Vmod $\sim 1 \times 10^{-12}$ $cm^3/cm^3$) are located within the root-mean-square interval. In particular, a high correlation (r = 0.85) was found between the model and lidar data between $10^{-12}$ and $10^{-10}$ $cm^3/cm^3$ (the correlation is statistically significant within the 0.05 level). Alternatively, below the $1 \times 10^{-12}$ $cm^3/cm^3$ threshold (i.e., the left of this vertical line) all points are located outside the root-mean-square interval. From the model simulations point of view, this unambiguously means that predicted dust volumes (Vmod, along the $x$ axis) lower than $1 \times 10^{-12}$ $cm^3/cm^3$ are not reliable.

[31] Similar results can be seen in Figure 5b for maximum dust volumes, even though the deviation of points from the bisector in this scatterplot is larger. In the overlapping range of model-lidar results, which is in Figure 5b between $10^{-12}$ and $10^{-9}$ $cm^3/cm^3$, the correlation between model and lidar data is equal to 0.51. Considering the whole dust vertical profile (Figure 5c), this comparison reveals that for points with Vmod greater than the threshold of $1 \times 10^{-12}$ $cm^3/cm^3$, the correlation coefficient between lidar data and the model-predicted ones is lower (r = 0.37); predicted dust volumes lower than $1 \times 10^{-12}$ $cm^3/cm^3$ are not trustworthy. In order to specifically evaluate the capability of the model results to correspond with lidar soundings near the top, bottom and middle parts of dust layers, three different symbols were used in Figure 5c: triangles corresponding to points at altitudes below 1.5 km, circles between 1.5 and 3.5 km and crosses above 3.5 km. One can see that the most remote points from the bisector correspond to crosses. Conversely, as expected, we get more accurate forecasts in the middle part of dust layers. Furthermore, in all scatterplots (Figures 5a–5c), the majority of points are located above the bisector. This means the model has a tendency to underestimate lidar-derived data.

[32] Figure 5 also highlights that the inaccurate forecast is not due to the weakness of dust events. In particular, even if Vobs in Figure 5a is less than $1 \times 10^{-11}$ $cm^3/cm^3$, there are accurate forecast points (with Vmod greater than the threshold of $1 \times 10^{-12}$ $cm^3/cm^3$) which correspond approximately to the same lidar-derived values as the inaccurate forecast points (with Vmod less than the threshold). A more thorough examination revealed that the inaccurate forecasts were associated with cloudiness over the area where the initial 3-D dust distribution had been obtained (with the aid of TOMS indices on the day previous to the forecast).

[33] As an example, accurate and inaccurate forecasts for two different days (see the two points in Figure 5a indicated by the arrows) in the month of May (17 May 2001 and 12 May 2003) are jointly analyzed in Figure 6. In accordance with Table 2, for both these days the lidar-derived dust volumes, averaged within the dust layer over Rome, are approximately the same ($7.03 \times 10^{-12}$ $cm^3/cm^3$ and $7.54 \times 10^{-12}$ $cm^3/cm^3$) while the model-simulated ones differ significantly ($0.08 \times 10^{-12}$ $cm^3/cm^3$ and $10.03 \times 10^{-12}$ $cm^3/cm^3$, respectively). Figure 6a presents the SeaWiFS image of the Mediterranean area for the day previous to the bad forecast (i.e., 16 May 2001). One can see clouds between North Africa and Italy, which cover the area around the endpoints of 24-hour back trajectories (shown by the rectangle in Figure 6c). Initialized in this area, the model-simulated dust would subsequently be transported over Rome (the starting points of 24-hour back trajectories were taken at the bottom, middle, and top heights of the lidar-measured dust layer over Rome on the forecast day). According to the Earth Probe Total Ozone Mapping Spectrometer measurements (see http://daac.gsfc.nasa.gov), reflectivity values greater than 20% (Figure 6e) associated to relatively low TOMS aerosol indices (about 1.1–1.5 in Figure 6g) were observed in the area under discussion. Alternatively, the accurate dust forecast on 12 May 2003

**Figure 6.** (a and b) SeaWiFS image of cloudiness over the Mediterranean area, (c and d) 24-hour air mass back trajectories started over Rome together with (e and f) horizontal distribution of reflectivity and (g and h) aerosol indices based on the measurements made by the Earth Probe Total Ozone Mapping Spectrometer. (left) Day previous to the dust storm on 17 May 2001. (right) Day previous to the dust storm on 12 May 2003. The start points of 24-hour back trajectories were taken over Rome at the bottom, middle, and top heights of the lidar-measured dust layer. The rectangles, built around the endpoints of 24-hour back trajectories, indicate the region where dust, initialized with the aid of TOMS AI, would subsequently be transported over Rome.

was accompanied by cloudless conditions (Figure 6b), low TOMS reflectivity (less than 20% in Figure 6f), and high TOMS aerosol indices (more than 3 in Figure 6h) over the rectangular area (Figure 6d), where dust was initialized 24 hours before the forecast time.

[34] A similar approach of estimating the averaged TOMS reflectivity was therefore used in order to identify cloudy conditions for all the points in the above-discussed scatterplots of Figures 5a and 5b. In particular, in Figures 5a and 5b the open and solid circles correspond to the points with the averaged TOMS reflectivity <20% and ≥20%, respectively. It is clearly seen that the points with averaged reflectivity less than 20% correspond mainly to acceptable forecast points (within the root-mean-square interval). Conversely, shown by the solid circles in Figures 5a and 5b, the points with the averaged reflectivity greater than or equal to 20% correspond mainly to inaccurate forecast points (outside the root-mean-square interval).

## 4. Discussion

[35] It should be emphasized that a short-term prediction of 3-D dust distribution is a very complex task. This largely results from the lack of operative information on the initial 3-D dust distribution. In order to overcome this difficulty, daily available global-scale TOMS aerosol indices were used for model initialization. The quantitative comparison between the lidar-derived dust volume profiles over Rome and those predicted by the model, initialized with the aid of TOMS indices, showed that the model is capable of giving mainly accurate forecasts in the middle part of dust layers. It was found, however, that the model predictions tend to underestimate the dust volume values derived by lidar. Furthermore, inaccurate forecasts cannot be explained by the weakness of dust events. To better understand this outcome, discussion on the possible reasons causing such model underestimations is given in section 4.2. Moreover, to correctly interpret the lidar data, evaluation of the expected accuracy of the lidar dust volume estimates is given hereafter.

### 4.1. Lidar Measurements and Dust Volume Estimates Accuracy

[36] Uncertainties affecting lidar measurements depend on several factors as the level of background noise, the signal noise (depending on distance from the system), the accuracy of the molecular atmosphere employed to calibrate the lidar trace (molecular density error), the accuracy of the lidar ratio assumed in the signal inversion (transmission error) [e.g., *Russell et al.*, 1979]. In fact, both signal and background noise determines the random error associated to the lidar signal. For the dust affected profiles discussed in this study, such random error in daylight conditions is about 1% below 4 km, 8% in the range 4–6 km and up to 30% in the 6–8 km range. For the same altitude ranges, these percentages become 1%, 4% and 7%, respectively, for measurements performed in nighttime conditions.

[37] Climatological monthly mean atmospheric p and T profiles based on 10 years of radiosounding data (recorded 30 km west of the measurements site) are employed in the lidar inversion to calibrate the signal. Departures of the resulting climatological molecular density profiles with respect to the actual ones are typically within 5% (molecular density error).

[38] Specific investigations were performed to evaluate the quality of our inversion approach in terms of both aerosol optical and physical properties in dust load conditions. *Gobbi et al.* [2002] proved that the functional relationships adopted to derive the altitude-dependent lidar ratio (and thus invert the lidar signal, see section 2.1.1) gave an accuracy on the aerosol extinction retrieval within 22% in Saharan dust conditions (transmission error).

[39] An evaluation of the lidar derived aerosol physical properties in Saharan dust conditions was performed comparing lidar estimates of desert dust surface area (S) and volume (V) with simultaneous, colocated in situ measurements of S and V [*Gobbi et al.*, 2003]. Outcomes of that closure study show a slight lidar tendency to underestimate desert dust volume, with mean lidar in situ measurements discrepancies within 20%. Since that study was performed in the near range portion of the lidar trace (lidar levels < 500 m), we expect an additional random error to affect the farther ranges, accordingly with the daytime values given above (8% at 4–6 km and 30% at 6–8 km).

[40] It is also worth noticing that, as opposite to modelled profiles, in which dust particles are considered on their own, real aerosol profiles also include particles of different nature. Particularly at lower levels, contribution of these particles to the lidar signal is significant. Therefore, when some increase in depolarisation indicates dust to reach down to the planetary boundary layer (PBL) ($z \leq 2$ km), some mixing of Saharan dust with PBL aerosol is expected. In these conditions it is very difficult to evaluate the relative contribution of dust with respect to PBL aerosol and the volume estimate is performed assuming the lidar backscatter signal as fully generated by dust. Dust volume estimate in the PBL should therefore be considered as the upper limit of the real one. Such an effect is observed, for example, in the lidar profiles in Figures 2b, 2g, and 2h.

### 4.2. Sources of the TAU Model Errors

[41] There could be a few reasons for the model to underestimate dust volume: (1) accuracy of dynamic atmospheric parameter predictions, (2) the model initialization procedure by the TOMS AI, and (3) assumptions on dust sources and dust particle size.

#### 4.2.1. Accuracy of Modeled Meteorological Parameters

[42] Dust particles in the model are captured by the wind at the surface. Subsequently, they are raised to considerable altitudes in the troposphere by strong convective regimes developed over the desert and are transported by winds to the Mediterranean Sea and farther. Therefore accuracy of model-predicted atmospheric dynamic parameters is important in correctly modeling dust generation and transport. One can then suggest that the model underestimation of dust volume could be due to some significant errors in the forecast of meteorological fields. If this forecast is incorrect, we could find an explicit relationship between the prediction errors of dust and the errors of wind, pressure, and temperature.

[43] In order to check this suggestion, a verification of the 24-hour model forecast of several atmospheric parameters was made. For this purpose, sea level pressure, geopotential heights at 500 hPa, temperature at 850 hPa, u and v wind

**Table 3.** RMSE Errors of the 24-Hour Model Forecast of Meteorological Fields Over the Region (25°N–45°N, 10°W–25°E), Averaged for Each Category[a]

| Type | SLP | H500 | T850 | U1000 | V1000 | U850 | V850 | U500 | V500 | dVave |
|---|---|---|---|---|---|---|---|---|---|---|
| I | 1.83 | 10.18 | 3.31 | 1.25 | 0.98 | 2.37 | 2.00 | 2.39 | 2.37 | 3.79 |
| II | 1.78 | 9.49 | 3.06 | 1.27 | 1.03 | 2.20 | 1.94 | 2.25 | 2.30 | 17.62 |
| III | 1.60 | 8.29 | 3.01 | 0.90 | 0.98 | 1.86 | 1.59 | 2.14 | 2.12 | 5.53 |
| IV | 1.69 | 11.65 | 2.45 | 1.15 | 1.24 | 2.27 | 1.90 | 2.47 | 2.26 | 55.70 |

[a]Definitions are as follows: SLP, for root-mean-square errors (RMSE) of the forecast of sea level pressure (hPa); H500, geopotential height (m); T850, temperature at 850 hPa (K); U1000, V1000, U850,V850, U500, and V500, u and v wind components at 1000, 850, and 500 hPa, respectively (m/s); dVave, absolute values of the difference between the lidar-derived averaged dust volume and that predicted by the model ($10^{-12}$ $cm^3/cm^3$).

components at 1000, 850, and 500 hPa were analyzed over the region 25°N–45°N, 10°W–25°E. This region was selected as the area over which dust can be transported for 24 hours by ~20 m/s velocity winds before reaching Rome. Root-mean-square errors (RMSE), between the forecast fields and the NCEP analysis were obtained for all 34 days under investigation. Averaged for each category, the RMSE of the selected parameters are presented in Table 3. One can see that the obtained RMSE are quite reasonable, meaning that the 24-hour model forecast of atmospheric parameters was acceptable for all dusty days under discussion. The accuracy of dust prediction was estimated as the absolute value of the difference between the lidar-derived averaged dust volume and the model-predicted one (dVave). No relationship was found between the dust errors and the RMSE estimates of meteorological fields, with correlation between them close to 0. Hence the RMSE of selected meteorological parameters is not correlated with dVave. Note that it would be also interesting to investigate the relationship between the errors of dust predictions and the errors of atmospheric parameters along the air mass backward trajectories ended in Rome. This relationship will be studied later.

#### 4.2.2. TOMS Initialization

[44] The issue of model initialization was discussed in detail by *Alpert et al.* [2002]. Three possibilities for the model initialization were examined, i.e., zero dust initialization, initialization with the previous dust model output, and initialization by TOMS AI data. The latter was shown to have an advantage over the others by four skill scores [*Alpert et al.*, 2002, Table 1]. Consequently, this approach was utilized in TAU short-term dust predictions, analyzed in the current study. However, some shortcomings of this approach should be taken into consideration.

[45] 1. TOMS does not detect dust overcastted by cloudiness. Moreover, aerosol indices could be contaminated by reflecting clouds, concurrently existing in the atmospheric column [*Torres et al.*, 2002]. Since Mediterranean dust transport is often associated with meteorological fronts, dust layers are frequently associated with clouds, causing incorrect model initializations.

[46] 2. The presence of both dust and nonabsorbing anthropogenic air pollution in the same atmospheric volume at the same time will lead to a reduction in the TOMS index. This factor may be of importance in the northern Mediterranean region, which suffers significantly from industrial pollution.

[47] 3. The TOMS AI is not sufficiently correct below 1 km, while above 1 km it is more reliable. *Herman et al.* [1997] found that UV-absorbing aerosols in the boundary layer near the ground could not readily be detected by the method used for AI calculation. This is due to the weak atmospheric signal near the ground relative to the apparent noise from the surface. However, *Torres et al.* [2002] consider this restriction not to be so important for mineral dust and suggest that the TOMS AI allow detection of dust particles even close to the ground.

[48] 4. The gridded (with horizontal resolution about 1°) data of TOMS aerosol indices were used to determine the initial 3-D dust distribution in the TAU model over each grid point of the model domain (with horizontal resolution of 0.5°). Of course, our comparison between gridded data and localized lidar measurements suggested in advance some discrepancy between them.

[49] 5. Owing to some uncertainties in the model capability to correctly simulate weak dust events, a restriction was made on dust initialization in those grid points where TOMS AI was less than 1. This restriction can be justified by the fact that over the Mediterranean region low TOMS aerosol indices are often due to the concurrent presence of nonabsorbing aerosols and/or reflecting clouds in the atmospheric column.

#### 4.2.3. Assumptions on Dust Sources and Particle Size

[50] As mentioned above (see section 2.2) the dust (clay) particles in the TAU prediction model were assumed to have one characteristic size with effective radius of 2–2.5 microns. This choice fitted the interval of dust particle sizes observed during long-range transport events of North Africa dust [*Levin et al.*, 1980; *Perry et al.*, 1997]. Later, *Alpert and Ganor* [2001] and *Israelevich et al.* [2003] showed that a wide range of dust particle sizes could be found in heavy dust storms over Israel, although 2–2.5 microns radius is within the interval of dominant sizes. Currently, however, most dust models employ 2 to 10 sizes of dust particles [*Kinne et al.*, 2003], in order to have better estimations of aerosol transport and radiative effects. One can then suspect that the dust particles used in the model could be too heavy for long-range dust transport. Our model simulations with different dust particle sizes are currently being carried out.

[51] Another reason for the model dust underprediction is that not all of possible dust sources in the Sahara desert are currently included in the model. The TAU model uses the *Ginoux et al.* [2001] topographical approach in order to determine appropriate low places within the Sahara desert which have a deep accumulation of alluvial sediments composed of fine particles that are easily eroded by wind. These low places are used in the model as dust sources. We found that indeed some dust sources in North Africa were missed in this approach: in particular, the sources over Tunis

and Libya that can be of importance for dust predictions over Rome.

## 5. Conclusions

[52] The lidar dust profiles over Rome presented in this study were collected in the 3-year period 2001–2003 during the high-dust activity season from March to June. These data were used for obtaining statistically significant reference parameters of dust layers such as the mean top and bottom heights and thickness. It was found that, on average, dust over Rome is distant from the surface and penetrates high into the troposphere up to 5–6 km. The lidar data were used to test the capabilities of the TAU short-term prediction model to correctly produce dust vertical distributions. Close inspection of the juxtaposed vertical profiles, obtained from lidar and model data near Rome, indicates that the majority (67%) of the cases under investigation can be classified as good or acceptable model forecasts of dust vertical distribution. A quantitative comparison between lidar-derived and model-predicted dust vertical profiles was also performed. To our knowledge, this is the first time this kind of long-term quantitative comparison is performed. The quantitative comparison showed that the model predictions are mainly accurate in the middle part of dust layers. This is supported by high correlation (0.85) between lidar and model data for forecasted dust volume greater than the threshold of $1 \times 10^{-12}$ $cm^3/cm^3$. The model, however, tends to underestimate the lidar-derived dust volume profiles. Possible reasons for the model underestimation have been analyzed. In particular, the TAU model initialization appears as one of the major problem of short-term dust forecasting. In those cases when the model-simulated dust concentrations were much lower than the observed ones, the largest role was found to be played by effect of clouds in the TOMS detection of aerosol indices (used to initialize the model). Moreover, some model assumptions on dust sources and particle size, and the accuracy of model-simulated meteorological parameters are also likely to affect the dust forecast quality.

[53] **Acknowledgments.** This research was supported by Israeli Space Agency (ISA) as part of the Mediterranean Israeli Dust Experiment (MEIDEX). The latter is a joint project between ISA and NASA. The study was also supported by the EU DETECT Project (contract EVK2-CT-1999-00048) and by the grant GLOWA-Jordan River. Lidar measurements employed in this study were partly supported by the Italian Space Agency (ASI) in the framework of the GASTRAN project. The authors thank Y. Kaufman and O. Torres for helpful discussion. We wish to acknowledge B. Starobinez, Z. Rosen, and S. Rechave for the encouragement and help. The remarks of anonymous referees improved the clarity of the paper, and we are grateful to them.

## References

Alpert, P., and E. Ganor (2001), Saharan mineral dust measurements from TOMS: Comparison to surface observations over the Middle East for the extreme dust storm, March 14–17, 1998, *J. Geophys. Res.*, *106*(D16), 18,275–18,286.

Alpert, P., and B. Ziv (1989), The Sharav cyclone: Observations and some theoretical considerations, *J. Geophys. Res.*, *94*(D15), 18,495–18,514.

Alpert, P., B. U. Neeman, and Y. Shay-El (1990), Intermonthly variability of cyclone tracks in the Mediterranean, *J. Clim.*, *3*, 1474–1478.

Alpert, P., S. O. Krichak, M. Tsidulko, H. Shafir, and J. H. Joseph (2002), A dust prediction system with TOMS initialization, *Mon. Weather Rev.*, *130*, 2335–2345.

Alpert, P., P. Kishcha, A. Shtivelman, S. O. Krichak, and J. H. Joseph (2004), Vertical distribution of Saharan dust based on 2.5-year model predictions, *Atmos. Res.*, *70*, 109–130.

Barnaba, F., and G. P. Gobbi (2001), Lidar estimation of tropospheric aerosol extinction, surface area and volume: Maritime and desert-dust cases, *J. Geophys. Res.*, *106*(D13), 3005–3018 (Correction, *J. Geophys. Res.*, *107*(D13), 4180, 10.1029/2002 JD002340, 2002.)

Barnaba, F., and G. P. Gobbi (2004), Modeling the aerosol extinction versus backscatter relationship for lidar applications: Maritime and continental conditions, *J. Atmos. Oceanic Technol.*, *21*(3), 428–442.

Bergametti, G., A. L. Dutot, P. Buat-Menard, R. Losno, and E. Remoudaki (1989), Seasonal variability of the elemental composition of atmospheric aerosol particles over the northwestern Mediterranean, *Tellus, Ser. B*, *41*, 353–361.

De Tomasi, F., A. Blanco, and M. R. Perrone (2003), Raman lidar monitoring of extinction and backscattering of Africa dust layers and dust characterization, *Appl. Opt.*, *42*, 1699–1709.

Di Sarra, A., T. Di Iorio, M. Cacciani, G. Fiocco, and D. Fuà (2001), Saharan dust profiles measured by lidar at Lampedusa, *J. Geophys. Res.*, *106*(D10), 10,335–10,348.

Ginoux, P., M. Chin, I. Tegen, J. M. Prospero, B. Holben, O. Dubovik, and S.-J. Lin (2001), Sources and distributions of dust aerosols simulated with the GOCART model, *J. Geophys. Res.*, *106*(D17), 20,255–20,274.

Gobbi, G. P., F. Barnaba, R. Giorgi, and A. Santacasa (2000), Altitude-resolved properties of a Saharan-dust event over the Mediterranean, *Atmos. Environ.*, *34*, 5119–5127.

Gobbi, G. P., F. Barnaba, M. Blumthaler, G. Labow, and J. Herman (2002), Observed effects of particles non-sphericity on the retrieval of marine and desert-dust aerosol optical depth by lidar, *Atmos. Res.*, *61*, 1–14.

Gobbi, G. P., F. Barnaba, R. Van Dingenen, J. P. Putaud, M. Mircea, and M. C. Facchini (2003), Lidar and in situ observations of continental and Saharan aerosol: Closure analysis of particles optical and physical properties, *Atmos. Chem. Phys.*, *3*, 2161–2172.

Gobbi, G. P., F. Barnaba, and L. Ammannato (2004), The vertical distribution of aerosols, Saharan dust and cirrus clouds at Rome (Italy) in the year 2001, *Atmos. Chem. Phys.*, *4*, 351–359.

Hamonou, E., P. Chazette, D. Balis, F. Dulac, X. Schneider, E. Galani, G. Ancellet, and A. Papayannis (1999), Characterization of the vertical structure of Saharan dust export to the Mediterranean basin, *J. Geophys. Res.*, *104*(D18), 22,257–22,270.

Herman, J. R., P. K. Bhartia, O. Torres, C. Hsu, C. Seftor, and E. Celarier (1997), Global distribution of UV-absorbing aerosol from Nimbus 7/TOMS data, *J. Geophys. Res.*, *102*, 16,911–16,922.

Intergovernmental Panel on Climate Change (2001), *Climate Change 2001—Impacts, Adaptation, and Vulnerability*, Cambridge Univ. Press, New York.

Israelevich, P. L., Z. Levin, J. H. Joseph, and E. Ganor (2002), Desert aerosol transport in the Mediterranean region as inferred from the TOMS aerosol index, *J. Geophys. Res.*, *107*(D21), 4572, doi:10.1029/2001JD002011.

Israelevich, P. L., E. Ganor, Z. Levin, and J. H. Joseph (2003), Annual variations of physical properties of desert dust over Israel, *J. Geophys. Res.*, *108*(D13), 4381, doi:10.1029/2002JD003163.

Janjic, Z. I. (1990), The step-mountain coordinate: Physical package, *Mon. Weather Rev.*, *118*, 1429–1443.

Kaufman, Y. J., D. Tanre, and O. Boucher (2002), A satellite view of aerosols in the climate system, *Nature*, *419*, 215–223.

Kinne, S., et al. (2003), Monthly averages of aerosol properties: A global comparison among models, satellite data, and AERONET ground data, *J. Geophys. Res.*, *108*(D20), 4634, doi:10.1029/2001JD001253.

Krichak, S. O., M. Tsidulko, and P. Alpert (2002), A study of an INDOEX period with aerosol transport to the eastern Mediterranean area, *J. Geophys. Res.*, *107*(D21), 4582, doi:10.1029/2001JD001169.

Levin, Z., J. H. Joseph, and Y. Mekler (1980), Properties of Sharav (Khamsin) dust—Comparison of optical and direct sampling data, *J. Atmos. Sci.*, *37*, 882–891.

Measures, R. M. (1984), *Laser Remote Sensing*, John Wiley, Hoboken, N. J.

Mesinger, E. (1997), Dynamics of limited area models: Formulation and numerical methods, *Meteorol. Atmos. Phys.*, *63*, 3–14.

Moulin, C., et al. (1998), Satellite climatology of African dust transport in the Mediterranean atmosphere, *J. Geophys. Res.*, *103*(D11), 13,137–13,144.

Müller, D., I. Mattis, U. Wandinger, A. Ansmann, D. Althausen, O. Dubovik, S. Eckhardt, and A. Sthol (2003), Saharan dust over a central European EARLINET-AERONET site: Combined observations

with Raman lidar and Sun photometer, *J. Geophys. Res.*, *108*(D12), 4345, doi:10.1029/2002JD002918.

Nickovic, S. (2003), DREAM dust model: Ongoing and future developments, paper presented at 2nd International Workshop on Mineral Dust, Inst. Natl. des Sci. de l'Univ., Paris, 10–12 Sept.

Nickovic, S., and S. Dobricic (1996), A model for long-range transport of desert dust, *Mon. Weather Rev.*, *124*, 2537–2544.

Olson, J. S., J. A. Watts, and L. J. Alison (1985), Major world ecosystem complexes ranked by carbon in live vegetation, *Carbon Dioxide Inf. Cent. Rep. NDP-017*, 288 pp., Oak Ridge Natl. Lab., Oak Ridge, Tenn.

Perry, K. D., T. A. Cahill, R. A. Eldred, and D. D. Dutcher (1997), Long-range transport of North African dust to the eastern United States, *J. Geophys. Res.*, *102*(D10), 11,225–11,238.

Prospero, J. M., P. Ginoux, O. Torres, S. Nicholson, and E. Gill (2002), Environmental characterization of global sources of atmospheric soil dust identified with the NIMBUS 7 Total Ozone Mapping Spectrometer (TOMS) absorbing aerosol product, *Rev. Geophys.*, *40*(1), 1002, doi:10.1029/2000RG000095.

Ramanathan, V., P. J. Crutzen, J. T. Kiehl, and D. Rosenfeld (2001), Aerosols, climate, and the hydrological cycle, *Science*, *294*, 2119–2124.

Rosenfeld, D. (2002), Suppression of rain and snow by urban and industrial air pollution, *Science*, *287*, 1793–1796.

Russell, P. B., T. J. Swissler, and M. P. McCormick (1979), Methodology for error analysis and simulation of lidar aerosol measurements, *Appl. Opt.*, *18*, 3783–3797.

Torres, O., P. K. Bhartia, J. R. Herman, A. Sinyuk, P. Ginoux, and B. Holben (2002), A long-term record of aerosol optical depth from TOMS observations and comparison to AERONET measurements, *J. Atmos. Sci.*, *59*, 398–413.

Tsidulko, M., S. O. Krichak, P. Alpert, O. Kakaliagou, G. Kallos, and A. Papadopoulos (2002), Numerical study of a very intensive eastern Mediterranean dust storm, 13–16 March 1998, *J. Geophys. Res.*, *107*(D21), 4581, doi:10.1029/2001JD001168.

P. Alpert, J. H. Joseph, P. Kishcha, S. O. Krichak, and A. Shtivelman, Department of Geophysics and Planetary Sciences, Tel Aviv University, Ramat Aviv, 69978 Tel Aviv, Israel. (kishcha@hotmail.com)

F. Barnaba and G. P. Gobbi, Istituto di Scienze dell'Atmosfera e del Clima, CNR, Via Fosso del Cavaliere 100, 00133 Rome, Italy.